# Chain Orientation in Melt-Extruded Samples of Vectra A, Vectra B, and Blends in Relation to the Mechanical Properties

S. DREHER,[1] S. SEIFERT,[1] H. G. ZACHMANN,[1] N. MOSZNER,[2] P. MERCOLI,[2] G. ZANGHELLINI[2]

[1] Institute for Technical and Macromolecular Chemistry, University of Hamburg, Bundesstraße 45, D-20146 Hamburg, Germany

[2] IVOCLAR AG, Bendererstraße 2, FL-9494 Schaan, Liechtenstein

*Received 10 July 1996; accepted 31 May 1997*

**ABSTRACT:** The profile of molecular orientation within injection-molded tensile bars of the liquid crystalline copolyesters Vectra A, Vectra B, and Vectra C, as well as blends of these polymers, was investigated by means of wide-angle X-ray scattering (WAXS) using synchrotron radiation (HASYLAB, Hamburg). The local variation of chain orientation was resolved into steps of 100 $\mu$m. An even higher resolution was obtained by using the microfocus camera (focal spot 2 $\mu$m) at the European Synchrotron Radiation Facility (ESRF) in Grenoble. In Vectra A and in the blend of Vectra A and Vectra B, a smooth variation of the orientation was found being almost zero at the surface and showing its maximum at a distance of 0.6 mm from the surface. The orientation in Vectra B was rather fluctuating. The average chain orientation in the blend samples processed under the same conditions was higher than in samples of the pure liquid crystalline copolyesters. The mechanical properties of the different layers within the injection moldings were determined by cutting the samples into slices and measuring the stress–strain curves. For specimens of comparable orientation, it turned out that the blend samples had the largest values of Young's modulus and tensile strength. The synergism of orientation and mechanical strength was also found for different blend compositions, as well as in blends of Vectra B and Vectra C. Annealing the injection moldings above the melting point resulted in a rapid relaxation of the orientation, whereas the chain alignment persisted at lower temperatures.  J Appl Polym Sci **67:** 531–545, 1998

## INTRODUCTION

Copolyesters of 6-hydroxy-2-naphthoic acid (HNA) and 4-hydroxybenzoic acid (HBA), as well as copoly(ester amide)s of 6-hydroxy-2-naphthoic acid, terephthalic acid (TA), and 4-aminophenol (AP), are promising, high-performance polymers known under the brand name of Vectra.[1] Vectra A (composed of 27% HNA and 73% HBA[2] and Vectra B (composed of 60% HNA, 20% TA and 20% AP[3] (Fig. 1) are of particular interest. Vectra C consists of the same monomers as Vectra A but exhibits an increased melting point of about 320°C and a reduced melt viscosity.

Generally, the mechanical properties of polymers are strongly influenced by the molecular order and orientation. This is valid for liquid crystalline polymers (LCP), in particular, as their rigid, rod-like chains can easily be oriented during extrusion. The morphology of Vectra A has been extensively examined by different authors.[4–9] This liquid crystalline copolyester crystallizes in a pseudo-

Dedicated to our friend and teacher Hans Gerhard Zachmann, who died on April 28, 1996.

*Correspondence to:* N. Moszner.

Journal of Applied Polymer Science, Vol. 67, 531–545 (1998)
 CCC 0021-8995/98/030531-15

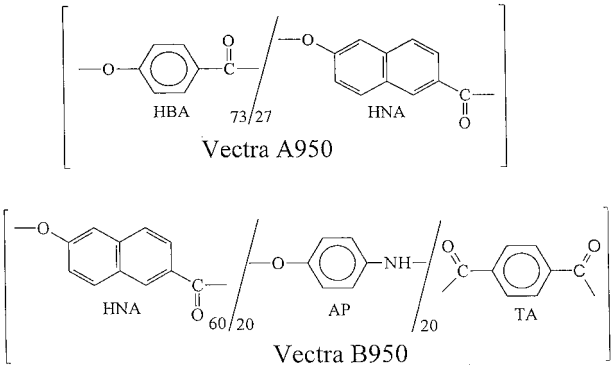


**Figure 1** Monomer units and molar ratios of Vectra A950 and Vectra B950.

hexagonal structure[10] and melts at about 300°C, thus being transformed into the liquid crystalline state. Just below the melting point, recrystallization effects occur upon annealing.[11–13] The investigation of the chain orientation in injection-molded tensile bars of Vectra A has shown[14–16] that the chains are preferentially oriented parallel to the extrusion direction. Nevertheless, the orientation strongly varies at different locations within the sample: close to the surface, the orientation is comparatively large; while it becomes much lower in the center of the sample.

Vectra polymers have often been used to reinforce conventional thermoplastics, such as PET,[17,18] PA,[19] PP[20,21] or ABS.[22] Coextrusion of these polymers with Vectra produces self-reinforced composites with improved mechanical properties. Nonetheless, the improved properties are often different from those predicted by the traditional "Rule of Mixture" because the mutual adhesion of the immiscible polymers is often very poor. The "Rule of Mixture" predicts the numerical values of properties, such as tensile and flexural strength, as well as tensile and flexural moduli, of a blend regarding the weighted average of the numerical values of the properties of the components.[23]

Contrary to these thermoplastic polymer blend systems, only very little is known about blends of two liquid crystalline polymers. The phase behavior of such blends is still being discussed.[24,25] For injection-molded blends of Vectra A and Vectra B with various compositions, Kiss[26] has found that the mechanical properties surpass those of each of the polymeric components of the blend if they are separately injection-molded. The reason for these synergetic effects of melt-blending on the mechanical properties is not yet fully understood.

The present article describes the chain orientation in injection-molded tensile bars of Vectra A, Vectra B, Vectra C, and of blends of the liquid crystalline copolyesters. The chain orientation of blend samples A/B and C/B is compared with the results for samples of the pure polymers. By using a particular geometry of the samples cut out of the injection moldings, we obtain the local distribution of the orientation with a resolution of 100 $\mu$m and less. Finally, the relation between the chain orientation and Young's modulus is determined in order to find the reason for the unexpectedly good mechanical properties of those blends. The results of solid-state nuclear magnetic resonance (NMR) investigations of the phase behavior of Vectra polymers will be presented in a forthcoming article.[27]

## EXPERIMENTAL

Vectra A, Vectra B, and Vectra C were purchased from Hoechst Celanese Co., Chatham, NJ. These polymers have an average molecular weight of about 20000 g mol. Blends of Vectra B with Vectra A and Vectra C, respectively, were obtained by coextrusion at 300°C using a twin-screw extruder. Blends A/B (1 : 3), A/B (3 : 2), and C/B (1 : 3) were investigated in particular. The numbers in parentheses represent the weight ratio of the two components. Dumbbell-shaped samples with the dimensions shown in Figure 2(a) were prepared by injection molding of the melt. The barrel temperature of the extruder was 290 ± 2°C with a residence time of the polymer melt in the mold of 20 s. The mold temperature was kept at 80 ± 2°C. The hydraulic injection pressure varied between

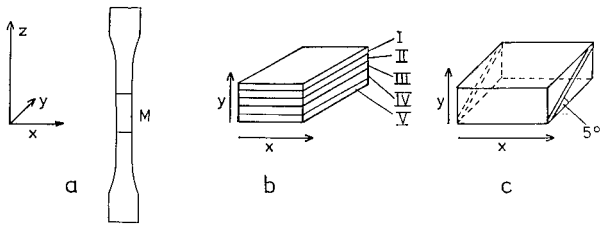


**Figure 2** Schematic representation of (a) the dumbbell-shaped samples according to ASTM tensile bars Type II: length, 15 cm; thickness, 4 mm; width in the center, 1 cm. Schematic representation of (b) the sheets, cut out of the middle part of the sample, designated by sheet I to V. Schematic representation of (c) the sheet diagonally cut under an angle of 5° with respect to the xz-plane out of the middle part of the sample.

2 and 11 MPa. If not stated otherwise, a pressure of 11 MPa was used.

In order to determine the local variation of the orientation and of the Young's modulus, the samples were cut into five slices numbered I to V, as indicated in Figure 2(b). The thickness of each slice was approximately 400 $\mu$m. Furthermore, a thin sheet (thickness 300 $\mu$m) was cut out of the sample with an angle of approx. 5° [Fig. 2(c)] in order to obtain a better local resolution in the WAXS measurements. As this specimen was not cut perpendicular to the sample surface, the different positions on the sheet are related to different distances from the surface of the tensile bar. Therefore, these diagonal cuts enabled us to record a quasicontinuous profile of molecular orientation by scanning the sheets with the X-ray beam. The resolution of this profile was limited only by the beam diameter and the thickness of the sheet.

The WAXS measurements were performed by means of a D500 Siemens $\vartheta/2\vartheta$-goniometer and using synchrotron radiation on the polymer beam line at HASYLAB (DESY, Hamburg). The measurements with a microfocus of 2 $\mu$m were carried out at the European Synchrotron Radiation Facility (ESRF) in Grenoble. For all synchrotron experiments, a two-dimensional Gabriel detector was used with the incident beam always perpendicular to the sample surface. In the measurements using the $\vartheta/2\vartheta$-goniometer, a normal counter was used. The incident angle of the beam varied with the scattering angle according to the $\vartheta/2\vartheta$-geometry.

For the evaluation of the molecular orientation the azimuthal intensity distribution $I(\phi)$ of the 110 crystal reflection at $2\vartheta = 19.7°$ (if Cu-$K_\alpha$ radiation is used) was analyzed. The Hermans orientation function $f$ of the chains can be calculated by using the following equations:

$$f = 1 - 3\langle\cos^2\phi\rangle \tag{1}$$

with

$$\langle\cos^2\phi\rangle = \frac{\int_{0°}^{90°} I(\phi)\sin\phi\,\cos^2\phi\,d\phi}{\int_{0°}^{90°} I(\phi)\sin\phi\,d\phi} \tag{2}$$

This equation was derived by Lovell and Mitchell[28] for the evaluation of reflections, which have their maximum on the equator and thus represent the orientation distribution of a vector that lies perpendicular to the chain axis. In case of a normal incidence beam geometry and a fixed position of the sample, $\langle\cos^2\phi\rangle$ has to be multiplied by $\cos^2\vartheta$ with $2\vartheta$ being the scattering angle in order to take the fact into account that the azimuthal angle $\phi$ on the film is not identical with the angle between the scattering net plane and the fiber axis (see Appendix). This procedure was applied in the present work.

**Table I Young's Modulus $E$ and Tensile Strength $\sigma_T$ of the Injection Molded Vectra Tensile Bars**

| Sample | $E$ (GPa) | $\sigma_T$ (MPa) |
|---|---|---|
| Vectra A950 | 6.6 | 150 |
| Vectra B950 | 12 | 111 |
| Vectra C950 | 8.3 | 155 |
| Vectra A/B (1 : 3) | 23.5 | 188 |
| Vectra A/B (3 : 2) | 16 | 230 |
| Vectra C/B (1 : 3) | 22 | 226 |

The Young's modulus $E$ and the tensile strength $\sigma_T$ were determined from stress–strain curves measured by means of an INSTRON testing machine. The overall stress–strain curves were obtained by using the original dumbbell-shaped samples. In order to gain further insight on the local variation of the mechanical properties, stress–strain measurements were carried out by using thin sheets (400 $\mu$m) cut out of the sample parallel to the surface, according to Figure 2(b). The length of each sheet was 3 cm.

Dynamic mechanical analysis (DMA) was performed to characterize the temperature dependence of the mechanical properties. The thin sheets cut out parallel to the surface [Fig. 2(b)] were examined with the DMA 983 from TA Instruments at a constant heating rate of 2°C per min. The glass transition temperatures of the various Vectra samples were determined from the maxima of the mechanical loss factor tan $\delta$ at the $\alpha$-relaxation.

## RESULTS

The values of the Young's modulus $E$ and fracture stress $\sigma_T$ obtained from for the original dumbbell-shaped samples are given in Table I. It is obvious that the blends of Vectra B with both Vectra A and Vectra C show higher values than do the pure components. These results correspond to mea-

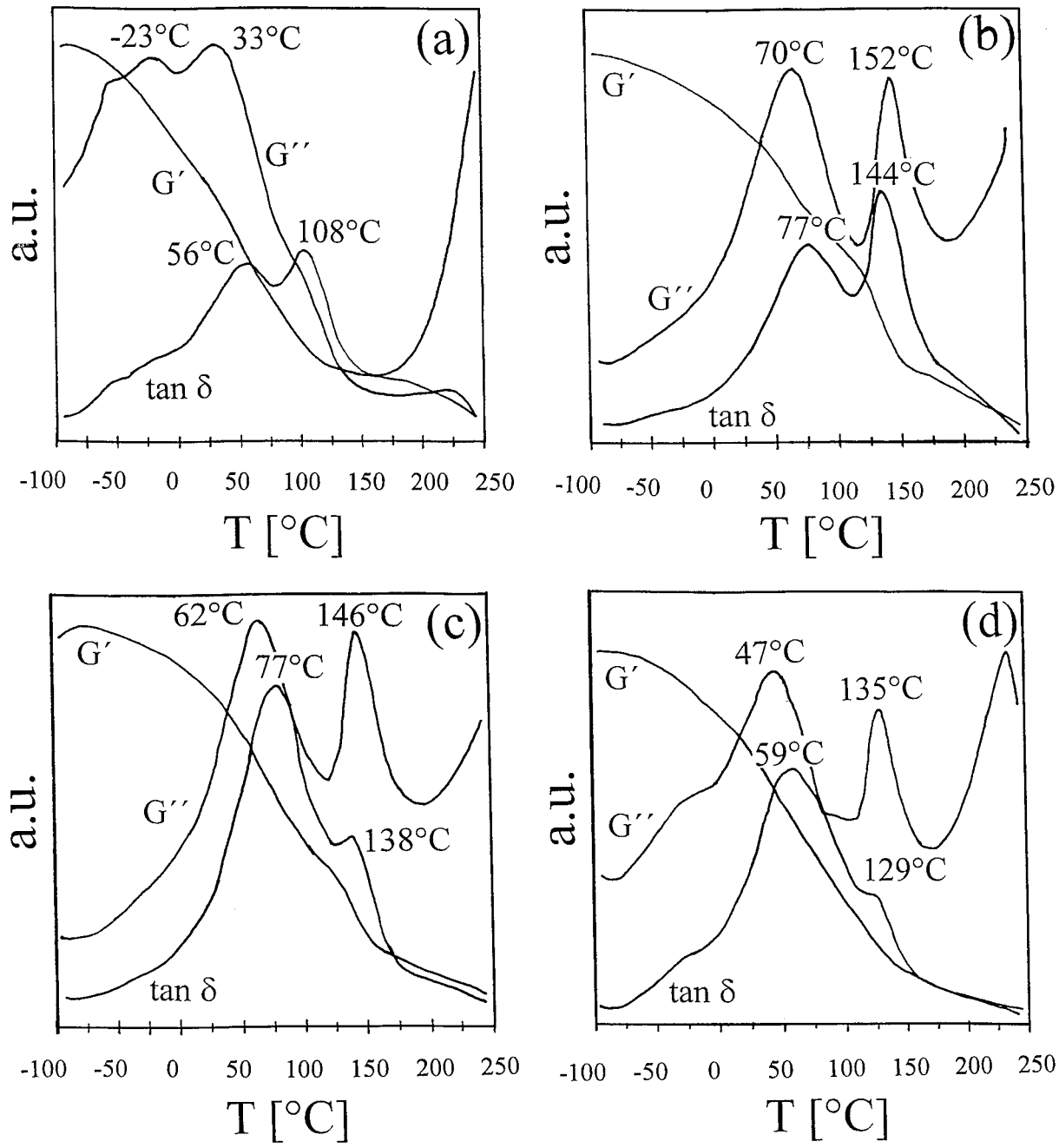


**Figure 3** Storage modulus G′, loss modulus G″, and loss factor tan $\delta$ as a function of temperature for (a) Vectra A, (b) Vectra B, (c) the blend A/B (1 : 3), and (d) the blend A/B (3 : 2).

surements of Kiss[26] and confirm the above-mentioned synergetic effect of melt-blending Vectra polymers on their mechanical properties.

The storage modulus $G'$, the loss modulus $G''$, and the loss factor tan $\delta$ for the two components and for the two blends of different compositions are shown in Figure 3. According to the maximum in tan $\delta$, Vectra A has a glass transition temperature of 108°C and Vectra B of 152°C. A single maximum in tan $\delta$ is found for each blend, which indicates that the blends are not phase-separated on a macroscopic scale. The glass transition is at 146°C for blend A/B (1 : 3) and at 135°C for blend A/B (3 : 2).

Young's modulus $E$ was determined from stress–strain curves of the samples of the blend

A/B (1 : 3) as a function of the pressure of injection molding. The results show (Fig. 4) that $E$ increases with pressure. The largest value obtained was 23.5 GPa. In comparison, the values obtained at the same pressure for Vectra A and Vectra B are 6.6 and 12 GPa, respectively. These results clearly confirm the influence of the processing parameters on the properties of the injection-molded parts. This is a fact one should always keep in mind when comparing samples. The difference in the mechanical properties is presumably caused by different degrees of molecular order and orientation within the samples. Hence, the following figures present the results of various scattering experiments to prove this assumption.

The WAXS intensity as a function of the scattering angle $2\vartheta$ of Vectra A, Vectra B, and the blend A/B (1 : 3) is shown in Figure 5. In order to exclude the effect of chain orientation, a powder of each material, obtained by milling the extruded samples, was used for this measurement. Very similar diagrams are obtained, which indicates that the molecular order is the same in all three materials.

The scattering patterns of Vectra A were obtained from sheet I (closest to the surface) and from sheet III (in the middle of the sample) (Fig. 6). It can be clearly recognized that the chains are highly oriented in sheet I, while the degree of orientation is much smaller in sheet III. Furthermore, the scattered intensity as a function of the scattering angle at the equator (perpendicular to the extrusion direction) and at the meridian (parallel to the extrusion direction) of sheet I of Vectra A, Vectra B, and blend A/B (1 : 3) (Fig. 7) shows

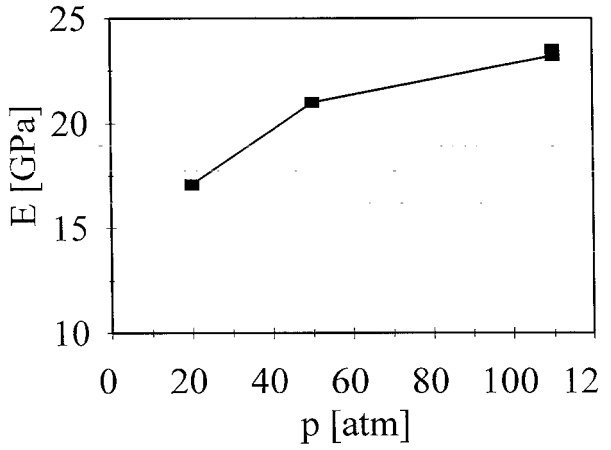


**Figure 4** Young modulus E of the dumbbell-shaped samples of the blend A/B (1 : 3) as a function of the hydraulic pressure $p$ during injection molding.

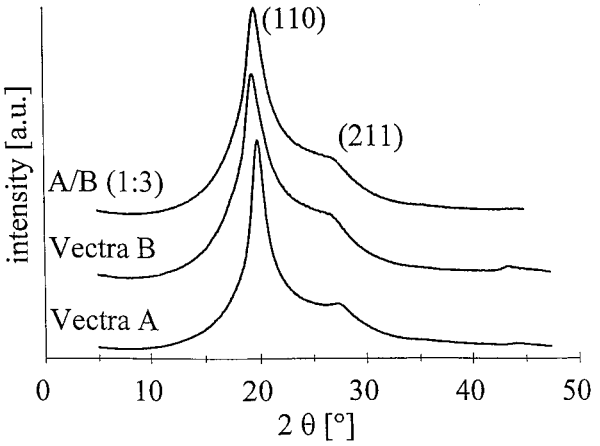


**Figure 5** Powder WAXS diagrams of Vectra A950, of Vectra B950, and of the blend A/B (1 : 3).

that a strong reflection appears at the meridian at about $2\vartheta = 38°$. This is probably due to the orientation of the chains. There is no reflection at the equator. However, the 110 reflection is much stronger at the equator than it is at the meridian. The relative intensities of the reflections demonstrate that the orientation in the blend is higher than it is in the components.

For the determination of the Hermans orientation function $f$ by means of eqs. (1) and (2), the contribution of air scattering, and of Compton scattering was subtracted. $\phi$ is the azimuthal angle, being zero at the meridian and 90° at the equator. After this subtraction, the question of further background subtraction arises. As an example, Figure 8 shows the azimuthal intensity distribution for Vectra A sheet I. Some authors[29] assume that there exists no contribution of the crystal reflection at an angle $\Delta\phi = 90°$ away from the maximum. For that reason, they subtract a background, as indicated by the dashed line in Figure 8 (method $\alpha$). This procedure is justified in case of high orientation and only if the orientation of the crystals is investigated. In our case, as shown in Figure 7, the 110 reflection does not completely disappear at the meridian ($\phi = 0$). Therefore, a more appropriate procedure to determine the background would be the one proposed by Blundell et al.[16] The scattered intensity $I$ is plotted as a function of the scattering angle $2\vartheta$ for different azimuthal angles $\phi$ (Fig. 9), and a straight line is drawn between the intensities at $2\vartheta = 10°$ and $2\vartheta = 35°$. From this line, the background of the 110 reflection at $2\vartheta = 19.7°$ is determined. This procedure is named as method $\beta$. As a third possibility, the intensity distribution as

**Figure 6** WAXS pattern of Vectra A950 obtained from sheet I (surface of the sample) and from sheet III (center of sample).

given in Figure 8 without any background subtraction (method $\gamma$) was used. This meant that the orientation of noncrystalline chains was also included into the evaluation to some approximation.

The Hermans orientation function $f$ of Vectra A measured for the sheets I, II, and III was obtained by applying all three different methods of background correction (Fig. 10). $f$ is plotted as a function of the distance $d$ from the surface. Because of the finite thickness of the sheets (400 $\mu$m), only an average value of the corresponding region is obtained. As expected, the larger the subtracted background, the higher the $f$ values. The crosses in Figure 10 represent the results obtained by Zülle et al.[15] with Vectra A sheets and background subtraction according to method $\alpha$. Fairly good correspondence was obtained.

Figures 11 and 12 depict the Hermans orientation function for the three sheets of Vectra B and blend A/B (1 : 3) in comparison with Vectra A. In agreement with the results represented in Figure 7, the highest orientation is found in the blend. Moreover, it is obvious that all samples show a drop-off in orientation from the skin to the core.

In order to obtain the local distribution of the molecular orientation with a higher resolution, WAXS measurements were performed on the diagonal cuts (Fig. 13). As was the case for the sheets, the material in the center of the sample ($d$ = 2 mm) was almost unoriented. For Vectra A and blend A/B, an increase of orientation was found at a distance between 0.4 and 1.4 mm from the surface. Close to the surface, the orientation decreases again. For Vectra B, the orientation seems to change more randomly.

Even more information can be obtained if the resolution is further enhanced by increasing the density of the points from which the scattering is measured (Fig. 14). For the samples of Vectra A and blend A/B, a smooth curve was obtained matching the orientation distributions found before. As a new result, however, it was found that the orientation at the surface of the sample is almost zero. In contrast, Vectra B shows a truly random fluctuation of $f$. This random fluctuation has been confirmed by the microfocus (2 $\mu$m) measurements (Fig. 15). In addition, these measurements revealed that not only the Hermans orientation function $f$ fluctuates, but also that the direction of main orientation varied by an angle $\beta$ of $\pm 40°$, as shown in Figure 15. The highest $\beta$-values occur in the center of the sample where the orientation is lowest. Obviously, the fluctuation in the orientation directions leads to a reduced net orientation. Figures 16 and 17 show the results of the microfocus measurements for Vectra A and blend A/B. For both samples, the smooth orientation distribution (Fig. 14) is confirmed. Moreover, these samples only showed slight fluctuations in the orientation direction ($\beta = \pm 12°$).

In addition to blend A/B (1 : 3), blend A/B (3 : 2) has been investigated. The orientation distribution obtained by WAXS measurements on the diagonal cuts shows a smooth orientation profile which has its maximum of about $f$ = 0.5 at

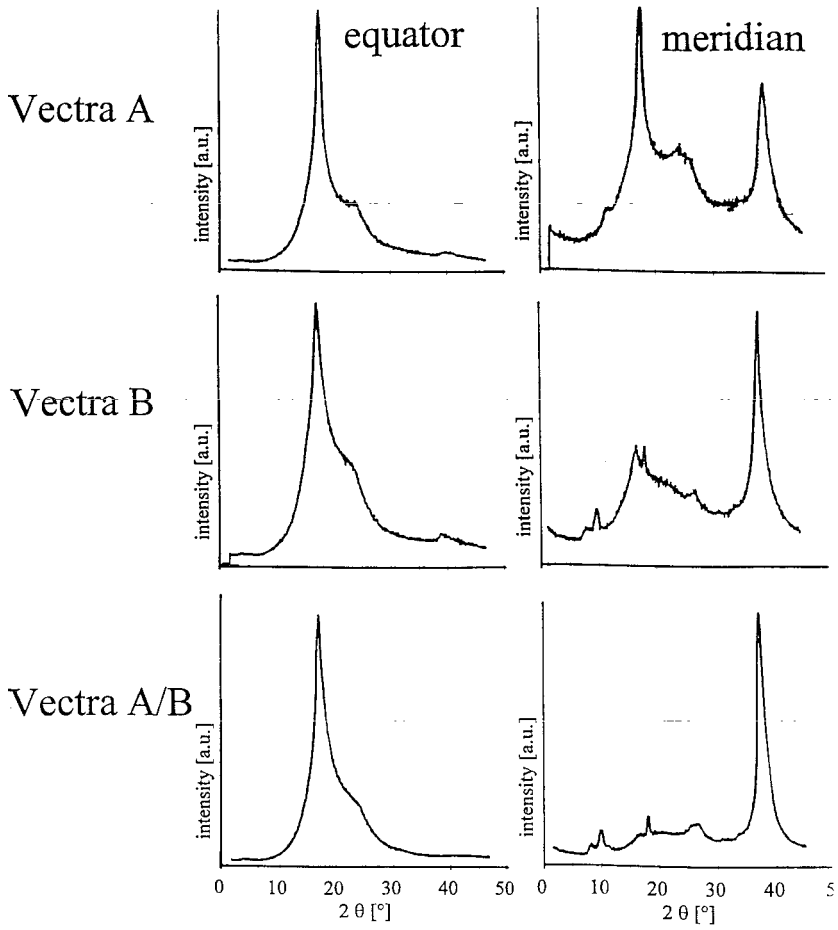


**Figure 7** Scattered intensity as a function of the scattering angle $2\vartheta$ on the equator and on the meridian of sheet I (surface sheet) of Vectra A, of Vectra B, and of the blend A/B (1 : 3).

about $d$ = 1 mm below the surface (Fig. 18). Towards the center, both samples evidence a drop-off in orientation. Towards the surface, the orientation of the Vectra-A-rich blend slightly decreases and levels off, whereas the orientation of the Vectra-B-rich blend continues to decline.

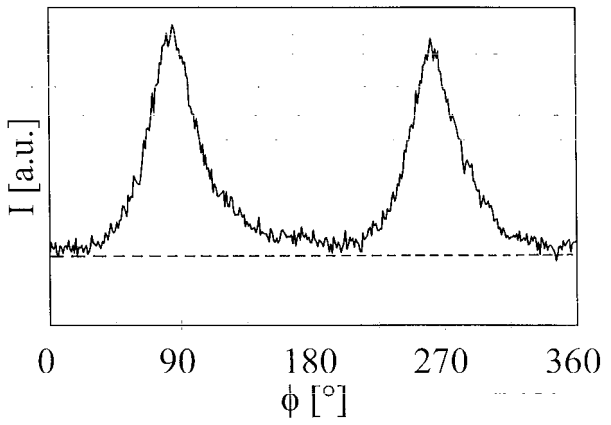


**Figure 8** Azimuthal intensity distribution of the 110 reflection at $2\vartheta$ = 19.7° obtained from sheet I of Vectra A.

An orientation distribution, which was somewhat different from the ones discussed above, was found in samples of Vectra C and of blend C/B (1 : 3) (Fig. 19). A minimum in the degree of orientation is reached at about $d$ = 1.2 mm rather than in the middle of the sample ($d$ = 2 mm). As for the blends containing Vectra A, the orientation of blend C/B (1 : 3) was higher than that of the pure components.

In order to relate the chain orientation to the Young's modulus, stress–strain curves of the different sheets cut parallel to the surface according to Figure 2(b) were measured. The Young's modulus $E$ as a function of the Hermans orientation function $f$ for the different materials confirms that higher orientation results in higher $E$ values (Fig. 20). Samples of Vectra B have higher moduli

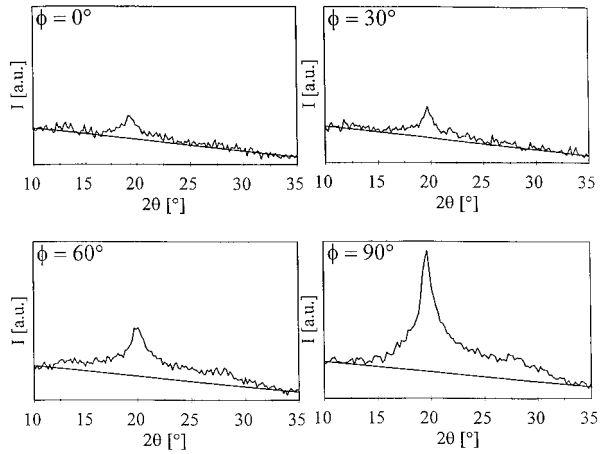


**Figure 9** WAXS intensity as a function of the scattering angle $2\vartheta$ for different azimuthal angles $\phi$ obtained from Vectra B. The straight line between $2\vartheta = 10°$ and $2\vartheta = 35°$ illustrates the background subtracted in method $\beta$.

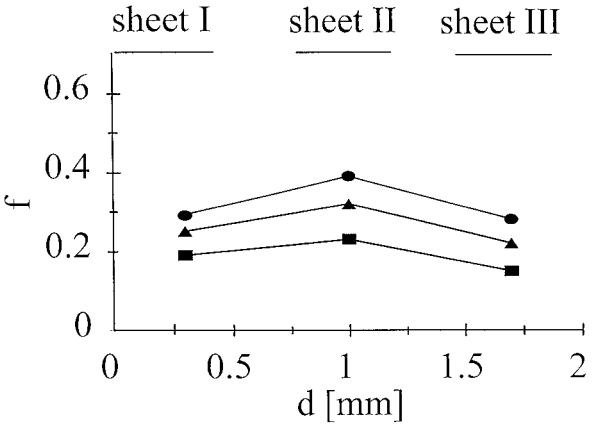


**Figure 11** Hermans orientation function $f$ of Vectra B as a function of the distance $d$ from the surface. The values have to be considered to be average values of sheet I, II, and III: (●) complete background subtraction (method $\alpha$); (△) background subtraction according to Figure 9 (method $\beta$); (■) without background subtraction (method $\gamma$).

than samples of Vectra A with the same orientation. This complies with the specifications of Hoechst–Celanese.[14] Young's moduli of blend samples A/B (1 : 3), however, are significantly higher than those of the samples of the individual components having the same degree of molecular orientation. These results suggest that the higher orientation of the blend samples is not the only reason for their superior mechanical properties. Rather, the inherent chemical structure obtained from blending two Vectra polymers has to be taken into consideration too.

In this context, it is also interesting to know how fast a relaxation of the molecular orientation takes place at elevated temperatures. This was examined by annealing thin sheets of the injection molding samples for different periods of time and determining the retained degree of orientation by WAXS measurements. Figure 21 depicts the azimuthal intensity distribution of the 110 reflection

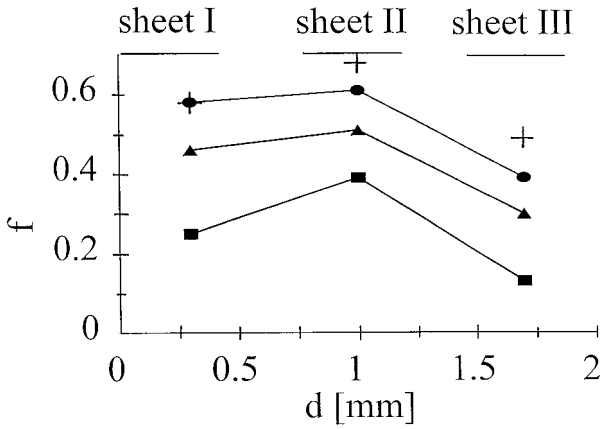


**Figure 10** Hermans orientation function $f$ of Vectra A as a function of the distance $d$ from the surface. The values have to be considered to be average values of sheet I, II, and III: (●) complete background subtraction (method $\alpha$); (△) background subtraction according to figure 9 (method $\beta$); (■) without background subtraction (method $\gamma$). The crosses represent the results obtained by Guiterrez et al.[8]

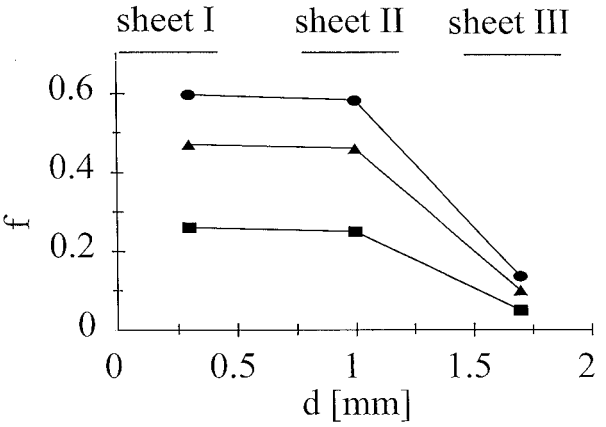


**Figure 12** Hermans orientation function $f$ of the blend A/B (1 : 3) as a function of the distance $d$ from the surface. The values have to be considered to be average values of sheet I, II, and III: (●) complete background subtraction (method $\alpha$); (△) background subtraction according to Figure 9 (method $\beta$); (■) without background subtraction (method $\gamma$).

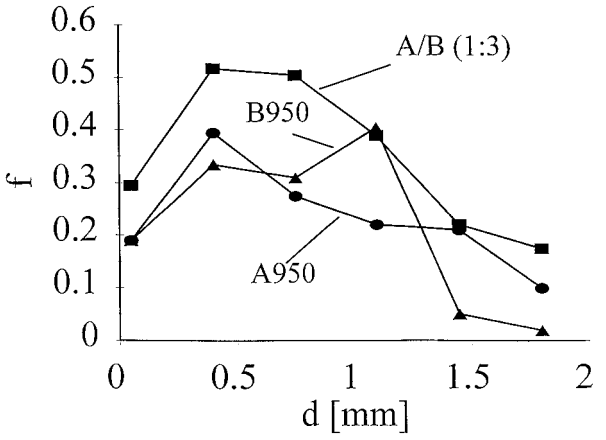


**Figure 13** Hermans orientation function $f$ as a function of the distance $d$ from the surface obtained from a diagonally cut sheet [see Figure 1(c)] of Vectra A950, Vectra B950, and the blend A/B (1 : 3), respectively. The distance of points corresponds to 350 $\mu$m in depth.

obtained from samples of the blend A/B (1 : 3) after annealing for different periods of time at 250 and 310°C, respectively. Annealing at 250°C, which is below the melting point, obviously only leads to a very slow decrease in orientation; whereas annealing at 310°C, which is within the range of melting, results in a relaxation within a few minutes. Annealing at temperatures above 320°C leads to an immediate relaxation. The decrease in orientation can be fitted by an exponential curve as the one shown in Figure 22. The relaxation times at 250 and at 310°C are 249 and 15 min, respectively.

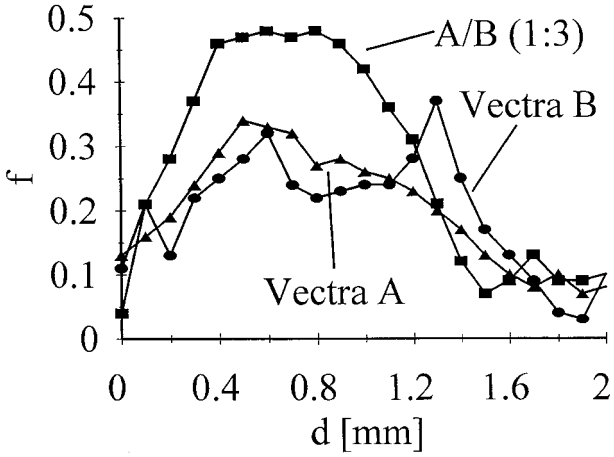


**Figure 14** Hermans orientation function $f$ as a function of the distance $d$ from the surface obtained from a diagonally cut sheet [see Figure 1(c)] of Vectra A950, Vectra B950, and of the blend A/B (1 : 3), respectively. The distance of points corresponds to 100 $\mu$m in depth.

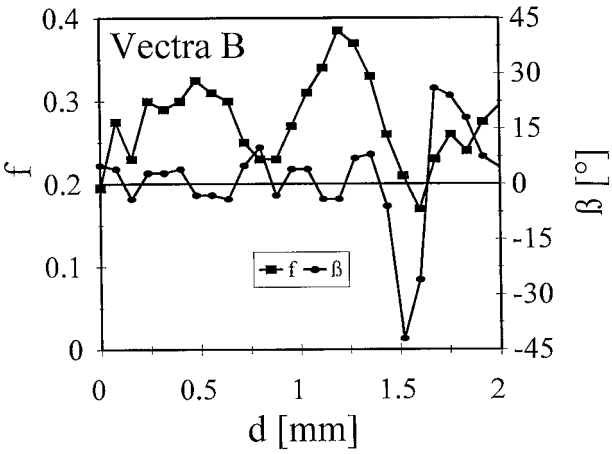


**Figure 15** Hermans orientation function $f$ and deviation $\beta$ of the direction of main orientation from the injection direction as a function of the distance $d$ from the surface obtained from a diagonally cut sheet [see Figure 1(c)] of Vectra B by means of a microfocus beam.

## DISCUSSION

### Orientation Distribution in Vectra A and Vectra B

The maximum of orientation found in Vectra A at a distance of about 0.8 mm from the surface is a well-known effect already found by means of various techniques.[16,30–34] By means of WAXS measurements of thin sheets similar to the ones in Figure 2(b), Plummer et al.[14] found values for the Hermans orientation function that resemble our results. Their birefrigence and microscopical measurements propose a five-layered structure,

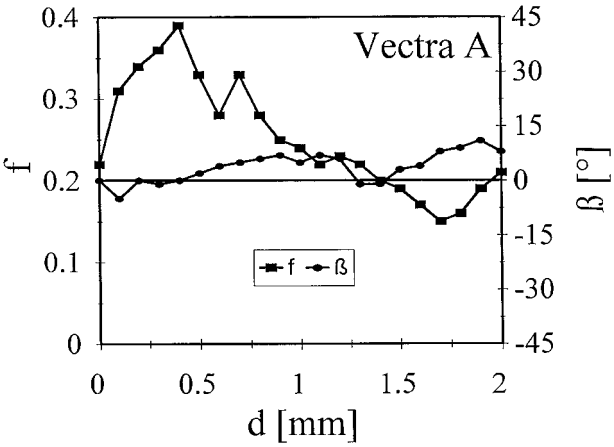


**Figure 16** Hermans orientation function $f$ and deviation $\beta$ of the direction of main orientation from the injection direction as a function of the instance $d$ from the surface obtained from a diagonally cut sheet [see Figure 1(c)] of Vectra A by means of a microfocus beam.

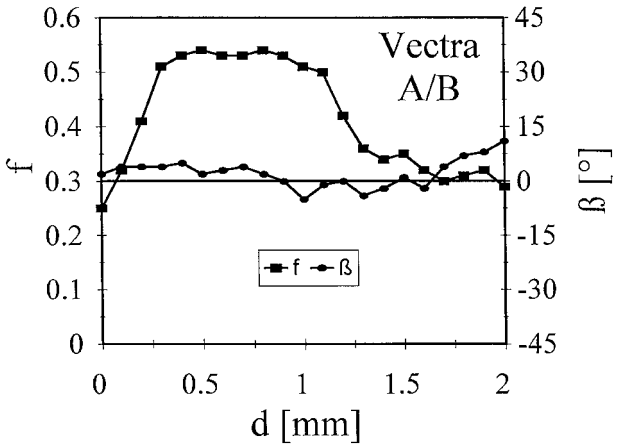


**Figure 17** Hermans orientation function $f$ and deviation $\beta$ of the direction of main orientation from the injection direction as a function of the distance $d$ from the surface obtained from a diagonally cut sheet [see Figure 1(c)] of the blend Vectra A/B (1 : 3) by means of a microfocus beam.

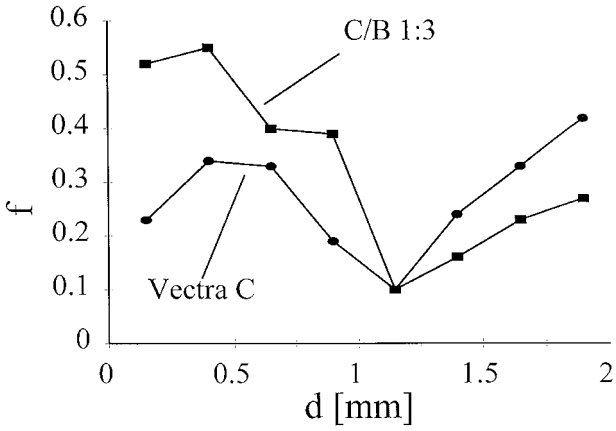


**Figure 19** Hermans orientation function $f$ as a function of the distance $d$ from the surface obtained from a diagonally cut sheet [see Figure 1(c)] of Vectra C and of the blend C/B (1 : 3), respectively.

with the outer skin layer being most oriented. In their opinions, the apparent disagreement with their X-ray data arises from differences in sample thickness, as mechanical measurements on sheets of 100 $\mu$m thickness reveal large fluctuations of the Young's modulus within the upper layers.

The highly resolved orientation distribution of the Vectra A and Vectra B samples examined in the present study also show a maximum of orientation at about 1 mm below the surface. However, these results clearly prove the existence of a less-oriented surface layer within the samples. Moreover, the microfocus WAXS measurements show that, only within samples of Vectra B, large fluctuations of the degree and direction of molecular orientation occur (Fig. 15). Therefore, the reason given by Plummer et al. for the apparent drop-off in orientation at the surface is not valid for the samples of Vectra A and blend A/B.

What is the reason for this discrepancy? The highly oriented sheet found by Plummer et al.[14] might have had a thickness much smaller than 40 $\mu$m so that it is not of considerable significance for our measurements. The sample thickness (300 $\mu$m) and the finite beam size (<500 $\mu$m) of the X-ray apparatus at DESY result in a decrease of the spatial resolution of the orientation profile. For the diagonally cut samples shown in Figure

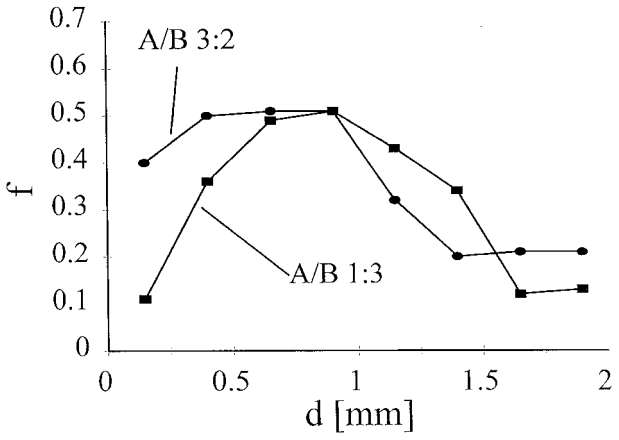


**Figure 18** Hermans orientation function $f$ as a function of the distance $d$ from a diagonally cut sheet [see Figure 1(c)] of the blends A/B (1 : 3) and A/B (3 : 2), respectively.

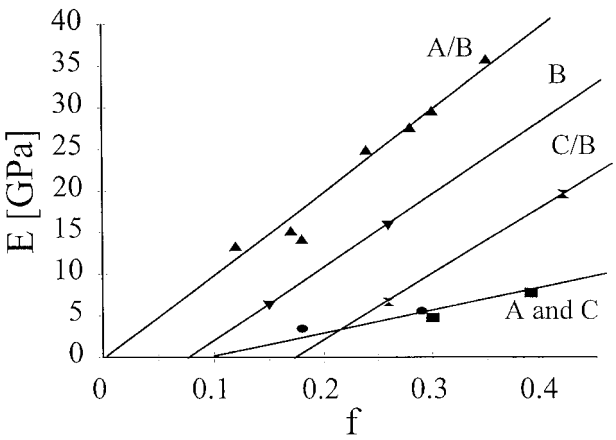


**Figure 20** Young's modulus E as a function of the Hermans orientation function $f$ obtained from the sheets cut parallel to the surface [Figure 2(b)] of various Vectra samples.

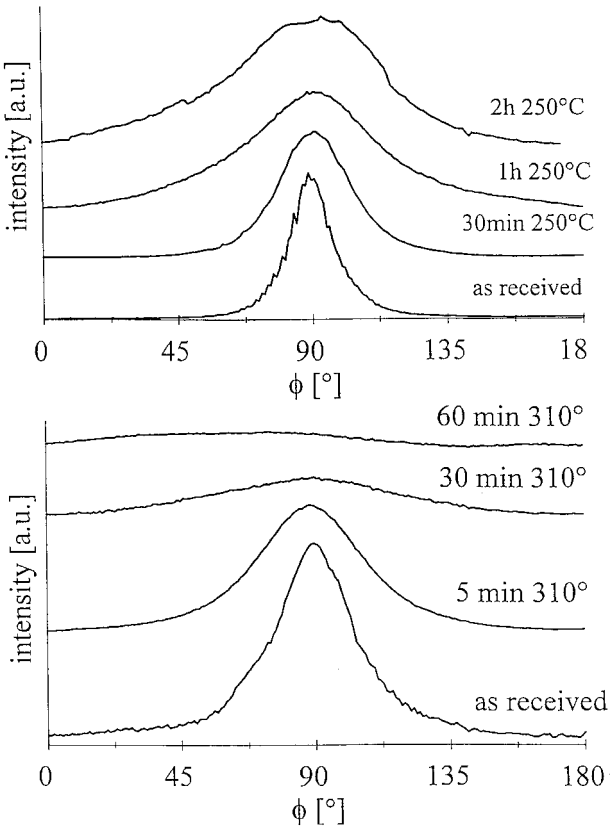


**Figure 21** Azimuthal intensity distribution obtained from sheets of the blend A/B (1 : 3) at a scattering angle of $2\theta = 19.7°$ after annealing for different times at 250 and 310°C, respectively.

2(c), we determined the average orientation of an about 40 $\mu$m thick layer, implying that thinner layers cannot be detected separately. As the thickness of the outer skin layer has been estimated by Plummer et al. to be approximately 40–50 $\mu$m, it is possible that the samples investigated in this study also contain a highly oriented, albeit thin, layer at the surface. In extrusion-molded samples of Vectra A, a highly oriented surface layer thinner than 20 $\mu$m was found by means of attenuated total reflection (ATR) infrared spectroscopy.[32] Further examinations by means of the microfocus camera will enable us to either confirm or reject the existence of a highly oriented, thin surface layer.

When discussing these differences, the fact that the processing parameters exert a profound influence on the microstructure of samples obtained from injection molding should also be mentioned. For instance, the thickness of the layer adhering to the mold wall during injection depends on the temperature of the mold and the melt, the injection pressure, and the distance from the inlet.[35] Figure 4 clearly demonstrates the dependence of the Young modulus on the pressure of injection. Recently, Sawhney et al.[22] showed very impressively the influence of processing conditions on the microstructure and mechanical properties of polyblends of Vectra A with an alloy of polyamide 6 and ABS. For that reason, only qualitative conclusions can be drawn by comparing orientation distributions of different injection-molded samples. This fact has to be kept in mind when discussing the results of different studies.

The fluctuation of the degree of orientation in samples of Vectra B is of particular interest. The very pronounced layer-like structure with large fluctuations in the degree and direction of orientation, especially in the center, is in sharp contrast to the smooth orientation profile of Vectra A and blend A/B. As all samples were prepared under the same conditions, the differences are attributed to inherent properties of the polymers, in particular to their rheological properties. It is a known fact that the orientation distribution within injection moldings is very sensitive to the flow history of the melt.[14]

Vectra A and Vectra B show no significant differences in their melt viscosities.[36] Nevertheless, a negative pressure coefficient ($dln\eta/dp$) was observed for Vectra B; whereas Vectra A shows the opposite behavior. By using different die diameters, Izu et al.[36] found that the molecular alignment upon shear is more pronounced for Vectra B than for Vectra A. Hence, Vectra B appears to be more sensitive to domain tumbling upon shearing.

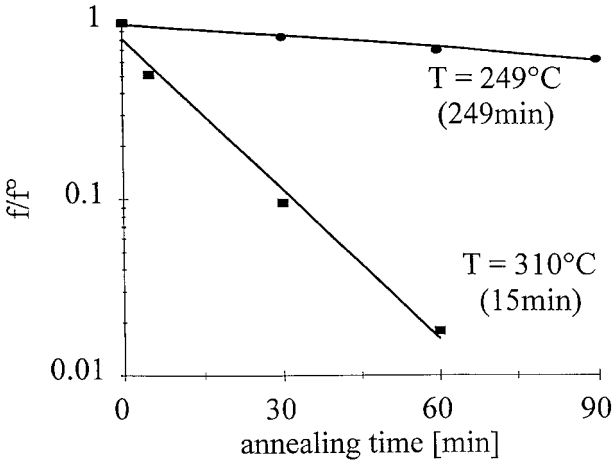


**Figure 22** Hermans orientation function $f$ obtained from the curves in Figure 19 as a function of the annealing time.

This may cause the orientation fluctuations and the formation of disclinations.[37] Moreover, the viscosity of Vectra B has a positive temperature dependence at elevated temperatures in the melt.[38] This peculiarity was not found for Vectra A. This effect, too, may be responsible for a different flow behavior of the two polymers leading to the different orientation profiles.

Studying the morphology of extruded and injection-molded samples of Vectra B, DéNève et al.[37] found three different textures, which they related to the applied shear strain and shear rate during processing. Near the surface, an ordered texture with a high degree of molecular alignment resulting from strong shear forces was observed. Reduced shear forces further inside the sample result in a wormlike texture with a high density of disclinations, while the center is characterized by a thread texture. These three textures correspond to the results of the microfocus X-ray measurements presented in Figure 15. The deviation of the direction of molecular alignment with respect to the direction of injection heavily fluctuates in the center of the sample, where the degree of orientation is comparatively low. According to the morphologies described above, the fluctuations can be attributed to a texture with a high disclination density and low degree of orientation, which can be called a wormlike texture. The high disclination density is confirmed by the fact that the difference in orientation determined with a conventional focus (Fig. 14) and a microfocus (Fig. 15) is particularly large in these layers. The molecular orientation in the submicron range is obviously much higher than the macroscopic orientation due to the presence of many defects in the director field.

The question arises as to how much the different glass transition temperatures are responsible for the different orientation profiles. Since Vectra A ($T_G$ = 100°C) has a lower glass transition temperature than Vectra B ($T_G$ = 150°C), the Vectra A samples will remain above $T_G$ longer than Vectra B samples during processing. Thus, there is more time to relax and to overcome orientation fluctuations by the annihilation of disclinations in Vectra A. However, the relaxation of molecular orientation can be neglected at temperatures below the melting point, as illustrated by the results in Figure 22. For this reason, the different glass transition temperatures will probably not influence the orientation profiles of the Vectra polymers.

### Orientation Distribution in Blend A/B (1 : 3)

According to previous investigations, Vectra A and Vectra B are thermodynamically immiscible. By long annealing at 320°C, however, a single phase system is formed as it was proved by $T_{1\rho}(^1H)$ measurements, polarization transfer nuclear magnetic resonance (NMR) investigations on blends in which one component was deuterated[27] and by the finding of a single glass transition (Fig. 3). Furthermore, NMR measurements of a solution of $^{13}C$-labeled blends showed that transesterifications took place during the annealing procedure. The single phase formation is enhanced by shearing during annealing. Viscosity measurements of a solution have shown that no significant change of the molecular weight during blending and extrusion has occurred in spite of the transesterifications. As Vectra A and B were blended by kneading and coextrusion, which involved annealing and simultaneous shearing, we conclude that blend A/B (1 : 3) forms a one-phase system, which consists of molecules being copolymers of Vectra A and Vectra B.

While the degree of orientation shows local fluctuations in Vectra B (Fig. 14 and 15), the change of the degree of orientation with increasing distance from the surface is rather smooth in blend A/B (1 : 3). The degree of orientation is almost zero at the surface; passes a maximum at a distance of 0.8 mm; and decreases again, approaching isotropy in the middle of the sample (Fig. 14). As the Vectra A homopolymer also shows a smooth local variation of the degree of orientation (Fig. 14), the smoothness of the blend is probably the result of Vectra A sequences in the copolymer.

The average value of the Hermans orientation function in blend A/B (1 : 3) is higher than the corresponding values of Vectra A and Vectra B processed under the same conditions. Rheological measurements show that the melt viscosity of the blend is somewhere between that of Vectra A and Vectra B. Therefore, the increase in orientation cannot be attributed to a change of viscosity. We believe that the increase is due to the smoother change in orientation caused by the presence of Vectra A units. These units seem to hinder the tumbling of the segments during flow, as discussed above.

### Orientation Distribution in Vectra C and in Blend C/B

The orientation profiles of Vectra C and blend C/B (1 : 3) have their minima at about 1.2 mm

from the surface. Further inside the sample, the orientation increases again up to $f$ values comparable to the ones of the upper layers. This second maximum may result from melt flow during the pressure stage[35] of the injection molding process. As the melt viscosity of Vectra C is rather low compared to that of Vectra A,[39] the flow behavior of these polymers during injection molding is supposed to be different, resulting in the different orientation profiles obtained.

### Young's Modulus

The Young's moduli $E$ of Vectra B, measured at the same value of the Hermans orientation function, are larger than the ones of Vectra A (Fig. 20). The Young's moduli of blend A/B (1 : 3) are even larger than those of Vectra B. While the difference between Vectra A and Vectra B may simply be a consequence of the different chemical structures, the increase observed after blending and transesterifying the two components requires further explanation. It is possible that differences in the local variations of the Hermans orientation function $f$ between the materials may be responsible for this result. While Vectra A shows a smooth variation of $f$ and comparatively small values of $E$, Vectra B shows larger values of $E$ which are, however, accompanied by local fluctuations of $f$ and $E$. These local fluctuations may prevent the Young's modulus $E$ from reaching high values. If this is true, this negative influence is removed by combining Vectra A and Vectra B, thus eliminating local variations of the orientation. Thus, in blend A/B (1 : 3), Vectra B contributes the high intrinsic values of $E$ and Vectra A is responsible for the necessary smoothness of the orientation profile.

It is interesting to note that the increase of molecular orientation by blending is also found in blends A/B (3 : 2) and C/B (1 : 3), as can be seen in Figures 18 and 19.

## CONCLUSIONS

In injection-molded tensile bars of Vectra polymers, it was found that the Young's modulus and the tensile strength are markedly high in blend material. This is valid for blends of Vectra A and B, as well as for blends of Vectra C and Vectra B. In order to understand these results, the molecular orientation within the injection-molded parts was examined by means of X-ray measurements. By cutting particular samples out of the tensile bars, the orientation profile perpendicular to the injection direction could be resolved.

In samples of Vectra A, a maximum in orientation was found at about 1 mm below the surface. The core of the samples is much less oriented, approaching isotropy. Towards the surface, a drop in orientation was observed, in contrast to previous samples.

The molecular orientation in samples of Vectra B is partly higher compared to that of Vectra A. The orientation profile, however, comprises strong fluctuations. Microfocus X-ray investigations revealed that the degree of orientation, as well as the direction, are fluctuating, especially in the core region of the sample. These results are in agreement with morphological studies,[37] revealing a wormlike texture with a high density of disclinations in the interior of injection-molded parts of Vectra B. The orientation profiles of Vectra A and Vectra B can be related to the different flow behavior of the two polymers resulting from their different chemical compositions.

In parts of blend A/B, a smooth orientation profile was found, similar to the one of Vectra A. The degree of orientation, however, is significantly higher in the blend material than in Vectra A and Vectra B. The more pronounced molecular alignment in the blend does not emerge from viscosity effects during blending but rather results from transreactions between the copolyester molecules of both blend components. The exchange reactions lead to the formation of a single phase blend consisting of copolymer molecules, which comprise segments of Vectra A and Vectra B. The high degree of orientation without any strong fluctuations of the orientation direction results in the high values of the Young's modulus and the tensile strength. Hence, the deviations from the "Rule of Mixture" are related to chemical and morphological changes during the blending process.

## APPENDIX

Let us consider a crystallographic net plane $P$ with the normal $n$ inclined by an angle $\gamma$ with respect to the symmetry axis $S$ of a sample showing axial symmetry (fiber symmetry). Because of the axial symmetry, all normals at this angle $g$ will intersect the sphere with the radius 1 in Figure A.1 on a circle $N$ with uniform density. However, according to Bragg's law, only those planes the normals of which will intersect the sphere on

the circle $R$ corresponding to half the Bragg angle will reflect the X-ray beam. Thus, in order to obtain scattering from these planes, the circles $R$ and $N$ have to intersect. This will be the case if

$$\gamma > \vartheta \tag{A.1}$$

In Figure A.1, this condition is fulfilled. $Q$ is one of the intersections. The angle $\phi$ indicated in Figure A.1 is the azimuthal angle (with respect to the meridian) under which the corresponding scattering point appears on a planar film $F$ behind the sample. This angle, however, is not identical with the angle $\gamma$ describing the direction of the normal, the squared cosine of which has to be averaged in order to calculate the Hermans orientation function. In case of a $\vartheta/2\vartheta$-goniometer $\gamma$ and $\phi$ would be identical.

In order to find a relation between $\phi$ and $\gamma$, we look at the projection represented in Figure A.2. From this figure, it follows that $\cos\gamma = a/1$ and $\cos\phi = a/\rho$. Figure 1 shows that $\rho = \cos\vartheta$. Thus,

$$\cos\phi = \frac{\cos\gamma}{\cos\vartheta} \tag{A.2}$$

If $h(\gamma)$ is the normalized probability to find an angle $\gamma$, we can write

$$\langle\cos^2\gamma\rangle = \int h(\gamma)\cos^2\gamma \sin\gamma \, d\gamma \tag{A.3}$$

If the relation given in eq. (A.1) holds for all net planes related to the considered Bragg angle $\vartheta$, the complete orientation distribution of these net

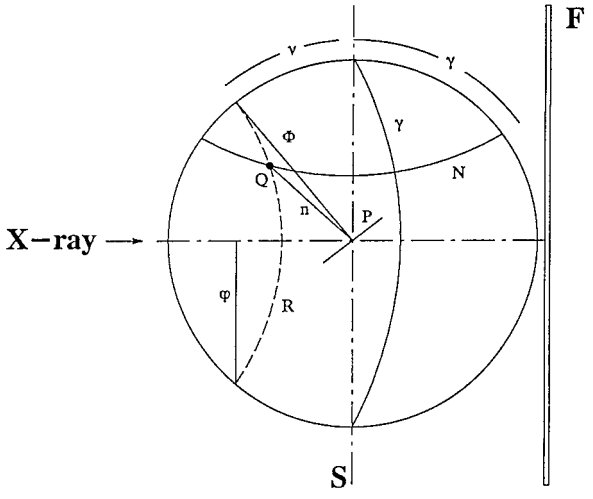


**Figure A.1**

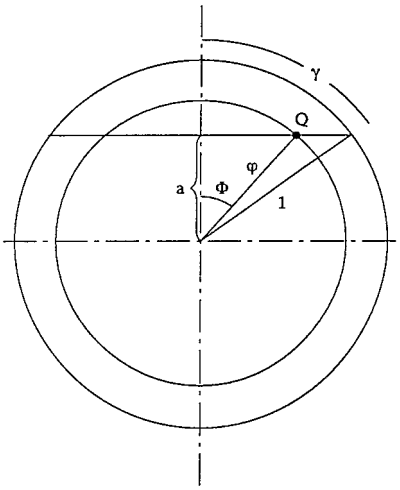


**Figure A.2**

planes is detected. Because of $h(\gamma)\sin\gamma\, d\gamma = I(\phi)\sin\phi\, d\phi$, one then obtains by means of eqs. (A.2) and (A.3),

$$\langle\cos^2\gamma\rangle = \cos^2\vartheta\,\langle\cos^2\phi\rangle \tag{A.4}$$

## REFERENCES


1. G. W. Calundann and M. Jaffe, in *Proceedings of the Robert A. Welch Foundation Conference on Chemical Research XXVI; Synth. Polym.,* Vol. 26, 1982, p. 247.
2. G. W. Calundann, U.S. Pat. 4,161,470 (1979).
3. A. J. East, L. F. Carbonneau, and G. W. Calundann, U.S. Pat. 4,330,457 (1982).
4. A. H. Windle, C. Viney, R. Golombok, A. M. Donald, and G. R. Mitchell, *Faraday Discuss. Chem. Soc.,* **79,** 55 (1985).
5. S. Hanna and A. H. Windle, *Polymer,* **29,** 207 (1988).
6. A. Biswas and J. Blackwell, *Macromolecules,* **21,** 3146 (1988).
7. A. Biswas, *J. Polym. Sci.,* **B30,** 1375 (1992).
8. G. A. Guiterrez, R. A. Chivers, J. Blackwell, J. B. Stamatoff, and H. Yoon, *Polymer,* **24,** 937 (1983).
9. J. Blackwell and A. Biswas, in *Developments in Oriented Polymers,* 2nd ed., I. M. Ward, Ed., Elsevier, New York, 1987.
10. D. J. Wilson, C. G. Vonk, and A. H. Windle, *Polymer,* **34,** 227 (1993).
11. Y. G. Lin and H. H. Winter, *Macromolecules,* **21,** 2439 (1988).
12. Y. G. Lin and H. H. Winter, *Macromolecules,* **24,** 2877 (1991).
13. A. Flores, F. Ania, F. J. Balta-Calleja, and I. M. Ward, *Polymer,* **34,** 2915 (1993).

14. C. J. G. Plummer, B. Zülle, A. Dermarmels, and H. H. Kausch, *J. Appl. Polym. Sci.,* **48,** 751 (1993).
15. B. Zülle, A. Dermarmels, C. J. G. Plummer, and H. H. Kausch, *Polymer,* **34,** 3628 (1993).
16. D. J. Blundell, R. A. Chivers, A. D. Curson, J. C. Love, and W. A. McDonald, *Polymer,* **29,** 1459 (1988).
17. M. S. Silverstein, A. Hiltner, and E. Baer, *J. Appl. Polym. Sci.,* **43,** 157 (1991).
18. W. G. Perkins, A. M. Marcelli, and H. W. Frerking, *J. Appl. Polym. Sci.,* **43,** 329 (1991).
19. A. Siegmann, A. Dagan, and S. Kenig, *Polymer,* **26,** 1325 (1985).
20. A. Datta, H. H. Chen, and D. G. Baird, *Polymer,* **34,** 759 (1993).
21. A. Datta and D. G. Baird, *Polymer,* **36,** 505 (1995).
22. G. Sawhney, S. K. Gupta, and A. Misra, *J. Appl. Polym. Sci.,* **62,** 1395 (1996).
23. L. E. Nielsen, *Mechanical Properties of Polymers and Composites,* Marcel Dekker, New York, 1974.
24. M. T. DeMeuse and M. Jaffe, in *Liquid Crystalline Polymers,* R. A. Weiss and C. K. Ober, Eds., ACS Symposium Series 435, 1990, Chap. 30.
25. M. T. DeMeuse and M. Jaffe, *Mol. Cryst. Liq. Cryst. Inc. Non-Lin. Opt.,* **157F,** 535 (1988).
26. G. Kiss, U.S. Pat. 4,567,227 (1986).
27. S. Dreher and H. G. Zachmann, to appear.
28. R. Lovell and G. R. Mitchell, *Acta Cryst.,* **A37,** 135 (1981).
29. G. R. Mitchell and A. H. Windle, *Polymer,* **24,** 1513 (1983).
30. S. Dreher and H. G. Zachmann, *Macromolecules,* **28,** 7071 (1995).
31. A. Kaito, M. Kyotani, and K. Nakayama, *J. Appl. Polym. Sci.,* **48,** 2147 (1993).
32. A. Kaito, M. Kyotani, and K. Nakayama, *J. Polym. Sci., Polym. Phys.,* **31,** 1099 (1993).
33. A. Kaito, M. Kyotani, and K. Nakayama, *Macromolecules,* **24,** 3244 (1991).
34. A. Pirnia and C. S. P. Sung, *Macromolecules,* **21,** 2699 (1988).
35. F. Johannaber, *Injection Molding Machines,* Hanser, Munich, 1983.
36. P. Izu, M. E. Muñoz, J. J. Peña, and A. Santamaria, *J. Polym. Sci., Polym. Phys.,* **31,** 347 (1993).
37. T. DéNève, P. Navard, and M. Kléman, *J. Rheol.,* **37,** 515 (1993).
38. J. M. Gonzalez, M. E. Muñoz, M. Cortazar, A. Santamaria, and J. J. Peña, *J. Polym. Sci., Polym. Phys.,* **28,** 1533 (1990).
39. *Vectra Polymere Werkstoffe,* Hoechst AG, 1992.